Simulation and control of dissolved air flotation and column froth flotation with simultaneous sedimentation

Raimund Bürger, Stefan Diehl, María Carmen Martí and Yolanda Vásquez

ABSTRACT

Flotation is a separation process where particles or droplets are removed from a suspension with the aid of floating gas bubbles. Applications include dissolved air flotation (DAF) in industrial wastewater treatment and column froth flotation (CFF) in wastewater treatment and mineral processing. One-dimensional models of flotation have been limited to steady-state situations for half a century by means of the drift-flux theory. A newly developed dynamic one-dimensional model formulated in terms of partial differential equations can be used to predict the process of simultaneous flotation of bubbles and sedimentation of particles that are not attached to bubbles. The governing model is a pair of first-order conservation laws for the aggregate and solids volume fractions as functions of height and time. An analysis of nonlinear ingredients of the governing equations helps to identify desired steady-state operating conditions. These can be chosen by means of operating charts, which are diagrams that visualize regions of admissible values of the volumetric flows of the feed input and underflow outlet. This is detailed for the DAF thickening process. Dynamic simulations are obtained with a recently developed numerical method. Responses to control actions are demonstrated with scenarios in CFF and DAF.

Key words | dissolved air flotation, multiphase flow, partial differential equation, separation, settling

Raimund Bürger (corresponding author)
Yolanda Vásquez
CI^{2}MA and Departamento de Ingeniería Matemática,
Universidad de Concepción,
Casilla 160-C, Concepción,
Chile
E-mail: *rburger@ing-mat.udec.cl*

Stefan Diehl
Centre for Mathematical Sciences,
Lund University,
P.O. Box 118, S-221 00, Lund,
Sweden

María Carmen Martí
Departament de Matemàtiques,
Universitat de València,
Avda. Vicent Andrés Estellés s/n, Burjassot, València,
Spain

HIGHLIGHTS

- Flotation processes with simultaneous sedimentation are simulated in one dimension.
- Three phases: aggregates (bubbles and hydrophobic material), solids and liquid.
- Control of steady states by operating charts for dissolved air flotation thickening.
- Model: system of nonlinear partial differential equations with user-defined constitutive functions.
- Extends former drift-flux theory of steady states to include dynamic behaviour.

INTRODUCTION

Gas flotation is a process to separate particles or droplets from a suspension when the particles/droplets are either too small or have a density too close to that of water to settle efficiently. The gas bubbles and particles/droplets form aggregates which rise to the top of a flotation tank where a layer of froth is skimmed off; see Figures 1 and 2 for two applications. The suspension may also contain hydrophilic particles that do not attach to bubbles and, if their density is larger than that of water, settle to the bottom where they are removed in the underflow.

Flotation is commonly used in industrial wastewater treatment to remove contaminants that are otherwise difficult to separate such as floating solids, residual chemicals, and droplets of oil and fat, and in mineral processing to recover valuable minerals (Finch & Dobby 1990; Rubio *et al.* 2002; Wang *et al.* 2007). For oil–water separation in wastewater treatment, there exist several induced and dissolved air flotation (DAF) technologies (Saththasivam *et al.* 2016); see also handbook entries (Wang *et al.* 2007: 71–99; Howe *et al.* 2012: 606; Metcalf & Eddy 2014:

doi: 10.2166/wst.2020.258

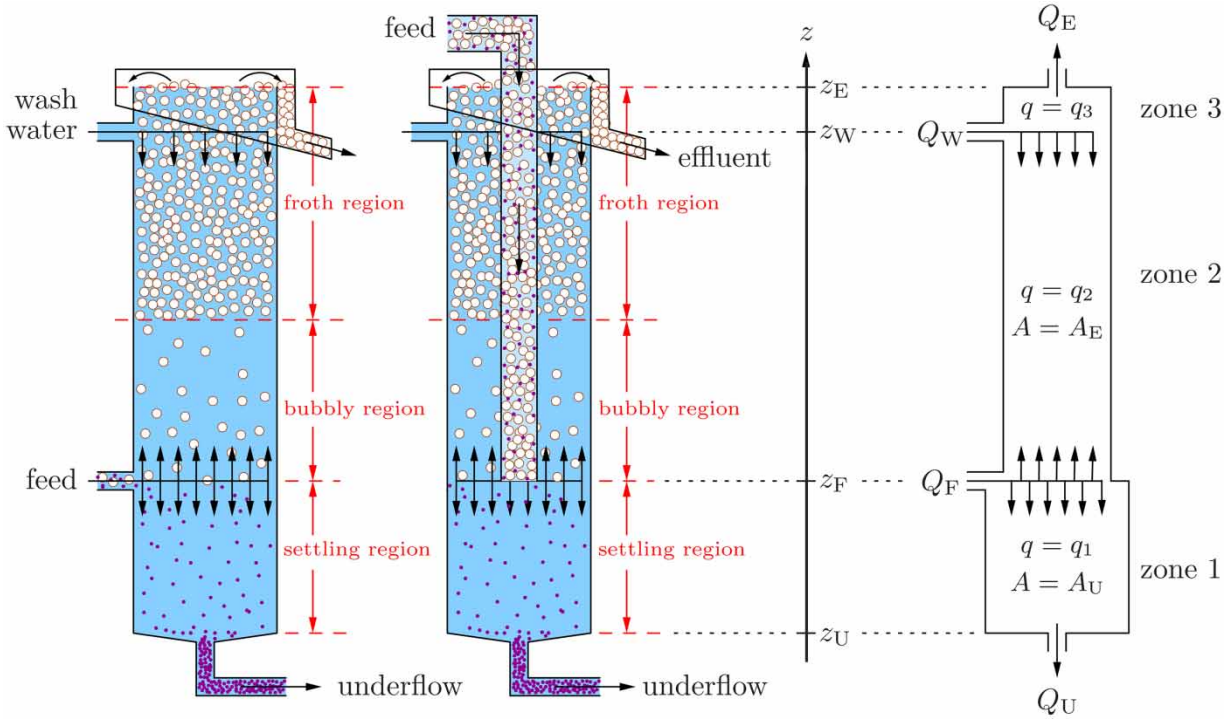

Figure 1 | Schematic of CFF with a feed inlet for slurry mixture and gas (cf. Bürger *et al.* 2019). At the top, wash water can be injected for desliming of unwanted particles. We simulate here the second column where the fluid–gas–particle slurry is fed through a downcomer pipe, which makes the cross-sectional area vary with height z.

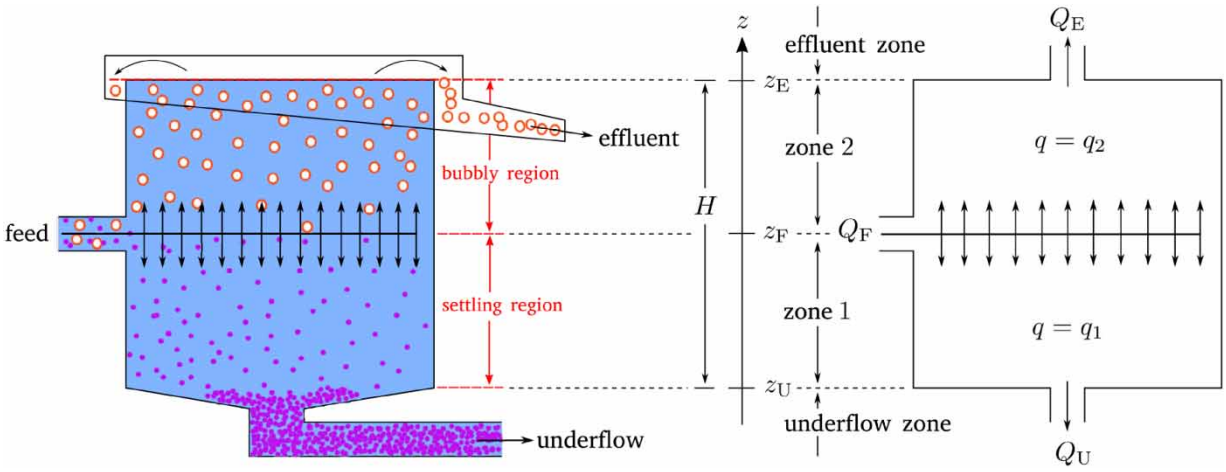

Figure 2 | Schematic of a DAF thickener (cf. Wang *et al.* 2007) with constant cross-sectional area and two zones.

403–408; Droste & Gehr 2019: 837–839). DAF has been used for many years for the thickening of waste activated sludge (WAS) (Butler *et al.* 1997; Chung & Kim 1997; Haarhoff & Bezuidenhout 1999). One of many advantages is that DAF can thicken sludge to concentrations at least a factor two higher than gravity settling (Reali *et al.* 2005; Wang *et al.* 2007). The flotation process is used for separating out either valuable or unwanted material at the top.

In column froth flotation (CFF), a stable foam or froth at the top is required; see Figure 1. This can be utilized in the removal of metal ions from wastewater (Beheir & Aziz 1996; Lin & Lo 1996; Rubio *et al.* 2002; Peng *et al.* 2018), removal of emulsified oil from wastewater (Chavadej *et al.* 2004), or recovery of riboflavin from wastewater (Qian *et al.* 2009). Another application is mineral processing, where valuable minerals are made hydrophobic, attach to the bubbles and

thereby form rising aggregates, while the hydrophilic gangue settles and is removed as tailings in the underflow (Finch & Dobby 1990); see Bürger *et al.* (2020) for further references. In the process of DAF thickening, no stable foam layer is needed; however, while WAS floats, grit and other substances may settle simultaneously (Butler *et al.* 1997; Wang *et al.* 2007); see Figure 2. Small air bubbles are trapped with the larger WAS flocs, which then float. In other applications, very small hydrophobic oil droplets attach to the air bubbles, while the grit settles. The simultaneous flotation–sedimentation process means that three phases are involved: liquid, buoyant aggregates and settling solids.

This contribution demonstrates that a new three-phase flow PDE (partial differential equation) model by Bürger *et al.* (2019) for one-dimensional (1D) modelling of simultaneous flotation and sedimentation can be utilized for different flotation applications with or without a layer of froth at the top. We refer to Bürger *et al.* (2019) for the derivation of the PDE model, the mathematical and numerical analyses behind the steady states and the numerical method. Our purpose is thus not to fit the model to specific data in a specific application. While Bürger *et al.* (in press) focus on the application to CFF in mineral processing, we present here new results for the DAF thickening process with the possible simultaneous sedimentation of solid particles. In particular, we present a new *operating chart* for the control of steady states of DAF thickening with sedimentation. The designs of flotation columns and DAF tanks are variable and since the purpose here is to advance a conceptual general model, we demonstrate its applicability to two different dimensioned tanks shown in Figures 1 and 2, and drift- and settling-flux functions in agreement with literature on CFF (Dickinson & Galvin 2014; Galvin & Dickinson 2014).

To put this contribution into the proper perspective, we mention that 1D models of flotation columns for the two-phase flow of aggregates and fluid have been based on the drift-flux theory (Wallis 1969; Dickinson & Galvin 2014), or empirical relationships (Bratby & Ambrose 1995), which can model steady-state situations only. Dynamic models of flotation are few in the literature. The two-phase PDE framework by Bascur (1991) is applicable to one of the zones of the column (Figure 1) and was extended (Bascur 2011) by several empirical equations for subprocesses, such as attachment and detachment in the froth and pulp regions. Cruz (1997) advanced a dynamic model of flotation with many ingredients, which is also based on the division of the tank into three regions: a collection region, a stabilized froth, and a draining froth. Those models incorporate numerous additional equations for subprocesses that require calibration of further parameters.

The present approach differs from the models referred to above. Apart from the tank dimensions, the only model inputs in our 1D model are two constitutive functions for the aggregate rise velocity and the particle sedimentation velocity, respectively. An advantage of this model is that the interfaces of pulp/froth and liquid/particles appear naturally as discontinuities in the solution and need not be tracked explicitly. The description of the rise of aggregates in a fluid is conceptually similar to the settling of particles described by a batch settling-flux function. Widely accepted dynamic 1D simulation models for continuous sedimentation based on PDEs have been developed since the 1990s (Diehl *et al.* 1990; Diehl 1996; Bürger *et al.* 2013). This contrasts with the case of flotation, for which the potential of 1D PDE-based models has not yet been exploited fully.

METHODS: PDE MODEL AND DYNAMIC SOLUTIONS

We assume that all aggregation of (hydrophobic) particles and bubbles occurs before the slurry is fed into the column, e.g. in the incoming pipe (Galvin & Dickinson 2014). This assumption is also consistent with the principle of operation of *dissolved* air flotation (i.e. there is one feed stream that also contains the air in dissolved form), as opposed to *dispersed* air flotation. The distinction between both is clearly made, for instance, by Metcalf & Eddy (2014). Figure 1 shows a typical vessel for froth flotation, where wash water can be injected at the top, while Figure 2 shows a DAF thickener which has no wash water. The conservation of mass for the three phases of aggregates, fluid and (hydrophilic) settling solids leads to the following system of PDEs (Bürger *et al.* 2019):

$$\frac{\partial(A(z)\phi)}{\partial t} + \frac{\partial(A(z)J(\phi, z, t))}{\partial z} = Q_{\mathrm{F}}\phi_{\mathrm{F}}\delta(z - z_{\mathrm{F}}), \tag{1}$$

$$\frac{\partial(A(z)(1-\phi)\varphi)}{\partial t} - \frac{\partial(A(z)F(\varphi, \phi, z, t))}{\partial z} = Q_{\mathrm{F}}\phi_{\mathrm{s,F}}\delta(z - z_{\mathrm{F}}). \tag{2}$$

The unknowns ϕ and φ depend on height z and time t. The volume fractions of aggregates are ϕ and solids ϕ_{s}, respectively. The variable $\varphi = \phi_{\mathrm{s}}/(1-\phi)$ is the volume fraction of settling solids within the suspension. The delta functions on the right-hand sides model the feed inlet at $z = z_{\mathrm{F}}$, where ϕ_{F} and $\phi_{\mathrm{s,F}}$ are the given volume fractions of aggregates and solids, respectively. The cross-sectional area

$A(z)$ may depend on z in any way; however, for the scenarios here we let it be piecewise constant and take at most two values (A_U and A_E); see Figure 1. With the given inlet volumetric flows Q_F and Q_W, we then define the zone bulk velocities $q_1 = -Q_U/A_U$, $q_2 = (-Q_U + Q_F)/A_E$ and $q_3 = (-Q_U + Q_F + Q_W)/A_E$ for CFF (Figure 1). For DAF (Figure 2), we let $A = A_U = A_E$. The total flux functions for the rising aggregates $J(\phi, z, t)$ and the settling solids $F(\varphi, \phi, z, t)$ are given by

$$J(\phi,z,t) = \begin{cases} q_3(t)\phi & \text{in effluent zone,} \\ q_3(t)\phi + j_b(\phi) & \text{in zone 3,} \\ q_2(t)\phi + j_b(\phi) & \text{in zone 2,} \\ q_1(t)\phi + j_b(\phi) & \text{in zone 1,} \\ q_1(t)\phi & \text{in underflow zone,} \end{cases}$$

$$F(\varphi,\phi,z,t) = \begin{cases} -(1-\phi)q_3(t)\varphi & \text{in effluent zone,} \\ (1-\phi)f_b(\varphi) + (j_b(\phi) - (1-\phi)q_3(t))\varphi & \text{in zone 3,} \\ (1-\phi)f_b(\varphi) + (j_b(\phi) - (1-\phi)q_2(t))\varphi & \text{in zone 2,} \\ (1-\phi)f_b(\varphi) + (j_b(\phi) - (1-\phi)q_1(t))\varphi & \text{in zone 1,} \\ -(1-\phi)q_1(t)\varphi & \text{in underflow zone.} \end{cases}$$

These total flux functions contain the batch drift-flux function $j_b(\phi)$ for the rising aggregates and the batch settling-flux function $f_b(\varphi)$ for the settling solids. Both functions principally have the same concave–convex form with one inflection point. The choice of explicit expression (polynomial, exponential, power law, etc.) for $j_b(\phi)$ and $f_b(\varphi)$ depends on the materials and belongs to the model calibration step. The choice does not influence the qualitative behaviour of the process. In fact, this contribution intends to provide insight to the qualitative behaviour of the process; specific numerical values are of minor interest. For the rising aggregates and for the settling particles, we use the following common batch flux functions (Richardson & Zaki 1954):

$$j_b(\phi) = v_{term}\phi(1-\phi)^n, \tag{3}$$

$$f_b(\varphi) = v_{term,s}\varphi(1-\varphi)^{n_s}, \tag{4}$$

where the terminal velocity of a single bubble in water is $v_{term} = 2.7$ cm/s and the dimensionless parameter n is chosen here as $n = 3.2$ (Dickinson & Galvin 2014). For the batch-settling flux $f_b(\varphi)$, we have chosen $v_{term,s} = 0.5$ cm/s (Scenario DAF1), $v_{term,s} = 0.1$ cm/s (Scenario DAF2), and $n_s = 2.5$. In the present model, we neglect, for simplicity, compression effects.

The PDE (1) contains only the unknown ϕ and this equation was analysed by Bürger *et al.* (2018). The analysis of the PDE system (1) and (2), which includes the settling of hydrophobic particles, is more involved; however, once Equation (1) is solved for $\phi = \phi(z, t)$ for a certain time period, Equation (2) can in principle be solved for φ as a scalar equation with $\phi(z, t)$ as a known function. We utilize this property in the classification of desired steady states for the derivation of operating charts and the numerical method for the PDE system. The latter has been adapted from a general treatment by Karlsen *et al.* (2009). The numerical method has been implemented in MATLAB (2019).

METHODS: STEADY STATES AND CONSTRUCTION OF AN OPERATING CHART FOR DAF

The analysis of the stationary solutions of (1) and (2) is delicate and invokes a so-called entropy condition (Diehl 1996) to obtain physically correct solutions. For given feed volume fractions ϕ_F and $\phi_{s,F}$, several nonlinear conditions on the volumetric flows have to be satisfied for a certain steady state to exist because of the feed inlets and discontinuities of the solution. The local maxima and minima of the zone flux functions appear in the inequalities (see Bürger *et al.* (2019) for all details). The nonlinear conditions can be visualized in operating charts (cf. Figures 3 and 6), where an operating point (Q_U, Q_F) in the admissible white region means that all conditions are satisfied. For CFF with wash water, the value of Q_W is calculated from a global mass balance. An operating chart depends on the values of ϕ_F and $\phi_{s,F}$, as can be seen from the difference between the left and right plots in Figure 3. We emphasize that the conditions for obtaining a certain steady state are only necessary; the actual state depends also on the dynamic history of the process.

By a desired steady-state solution in DAF thickening (where there is no wash water), we mean that aggregates are only present above the feed level and settling solids only below. The necessary conditions on the operating point (Q_U, Q_F) in the DAF case are four inequalities, which we now state and which are visualized in Figure 6. We assume, for simplicity, that the cross-sectional area A is constant. The fluid flow in zone 2 above the feed inlet should be upwards. This first constraint can be written as

$$Q_F - Q_U - Q_F\phi_F > 0 \tag{5}$$

and for given ϕ_F this means an (upper left) triangular region in the operating chart; see two such in Figure 6. For the derivation of (5), we refer to Bürger *et al.* (2019); see condition (FIIIa) therein. Condition (5) implies that the effluent

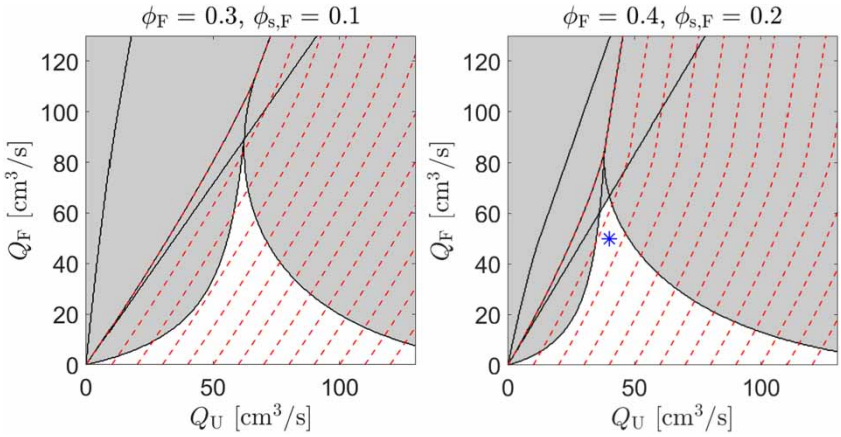

Figure 3 | Operating charts for CFF showing the intersection of several nonlinear inequalities for given feed volume fractions of aggregates ϕ_F and solids $\phi_{s,F}$. The white region shows the values of (Q_U, Q_F) that can be chosen to obtain a desired steady state. The top corner of the white region indicates the maximum possible value for Q_F, which is the optimal handling capacity. Along each dashed curve the volumetric wash water flow Q_W is constant and its value can be read off the Q_U-axis; i.e. on the leftmost curve $Q_W = 0$ cm^3/s, on the next one $Q_W = 10$ cm^3/s, etc.

volumetric flow satisfies $Q_E = Q_F - Q_U > 0$. The other three curves that define the white region in the operating chart are given by the following nonlinear inequalities (Bürger *et al.* 2019: conditions (FIa), (FIb) and (FIas)):

$$j_b(\phi_2^M(q_2)) + q_2\phi_2^M(q_2) \geq \frac{Q_F\phi_F}{A},$$

$$\phi_2 \leq \phi_{1Z},$$

$$f_b(\varphi_{1M}(q_1)) - q_1\varphi_{1M}(q_1) \geq \frac{Q_F\phi_{s,F}}{A}.$$

These formulas involve four volume fractions that are calculated as follows:

- $\phi_2^M(q_2)$ is the local maximum point (located below the inflection point) of the function $j_b(\phi) + q_2\phi$,
- ϕ_2 is the solution (located to the left of the maximum point $\phi_2^M(q_2)$) of the equation $j_b(\phi) + q_2\phi = Q_F\phi_F/A$,
- ϕ_{1Z} is the solution of the equation $j_b(\phi) + q_1\phi = 0$,
- $\varphi_{1M}(q_1)$ is the local minimum point (located to the right of the inflection point) of the function $f_b(\varphi) - q_1\varphi$,

where we recall that $q_1 = -Q_U/A$ and $q_2 = (-Q_U + Q_F)/A$.

RESULTS FOR CFF WITH WASH WATER

For the case study of CFF in Figure 1, we have used the values $A_E = 72.25$ cm^2 and $A_U = 83.65$ cm^2, and consider a laboratory scale column of height 1 m with $z_F = 33$ cm and $z_W = 90$ cm.

Two operating charts are shown in Figure 3 for a desired steady-state solution having a layer of froth in zone 3, a possible froth discontinuity in zone 2, and solids only in zone 1 (Bürger *et al.* 2019: case SS31).

Scenario CFF

We assume that the feed volume fractions are $\phi_F = 0.4$ and $\phi_{s,F} = 0.2$. In Figure 3 (right), we choose the operating point $(Q_U, Q_F) = (40,\ 50)$ cm^3/s in the white region; see the asterisk. The wash water volumetric flow is calculated to $Q_W = 14.46$ cm^3/s, which is the maximum that can flow downwards through the foam. A larger value would cause an overflow of wash water through the effluent. Figures 4 and 5 show a simulation when the column initially contains only water. Very quickly, a steady state is reached at $t = 180$ s; see Figures 4 (left) and 5(a). This has a low concentration of aggregates at the top and we perform some control actions. At $t = 180$ s, the top is closed until $t = 200$ s by temporarily setting $Q_U = 64.46$ cm^3/s (so that the effluent volumetric flow is $Q_E = 0$ cm^3/s). Aggregates will then accumulate at the top of the column and around the feed inlet. At $t = 200$ s, we reopen the effluent by setting back $Q_U = 40$ cm^3/s. The aggregates then move upwards; compare Figure 5(b) and 5(c). At about $t = 400$ s, an approximate steady state is reached (Figure 5(d)), which has a high concentration of froth only in the small zone 3. If we close the top of the tank again for 20 s more, another steady state is reached at about $t = 620$ s with a high froth concentration also in the upper part of zone 2, which is a desired steady state in mineral processing.

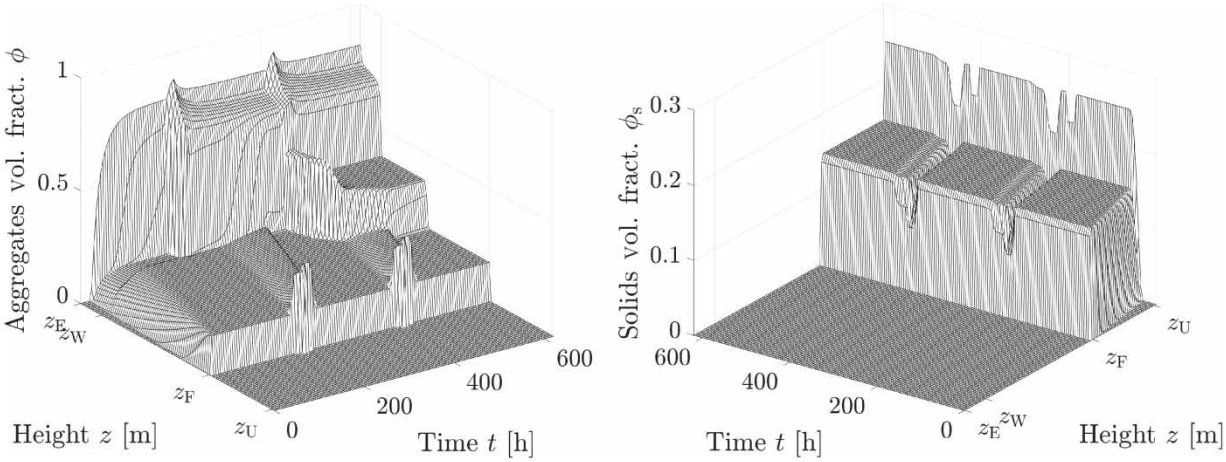

Figure 4 | Scenario CFF: simulation results with volume fractions of aggregates (left) and solids (right) as functions of height z [cm] and time t [s].

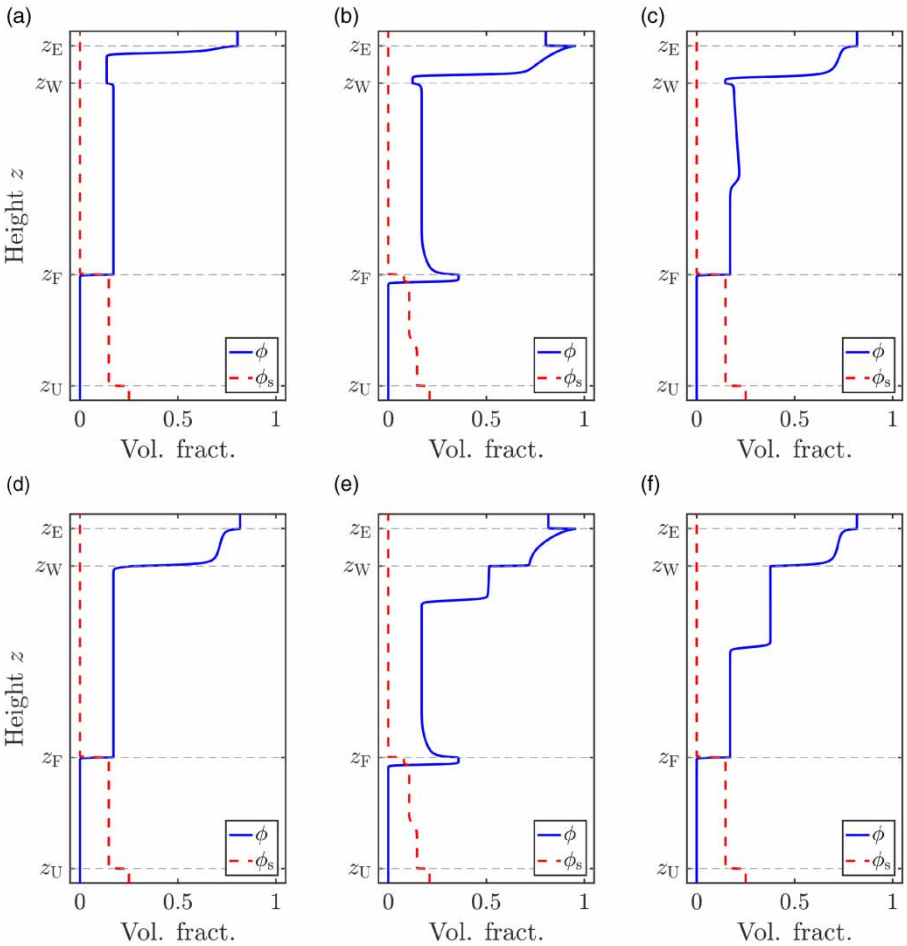

Figure 5 | Scenario CFF: snapshots of the simulation shown in Figure 4 at $t = 180$, 200, 300, 400, 420 and 620 s for the volume fractions of the aggregates ϕ_F (solid) and solids $\phi_{s,F}$ (dashed).

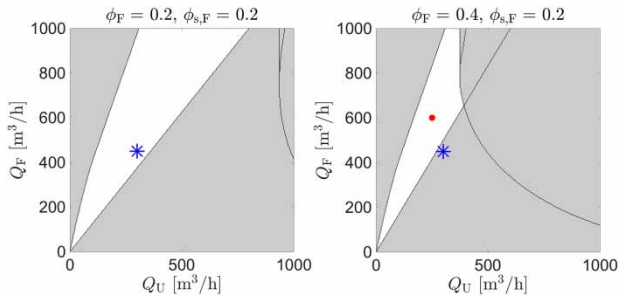

Figure 6 | Scenario DAF1: operating charts before $t = 0.27$ h = 16.2 min (left) and after (right), where the feed volume fractions ϕ_F and $\phi_{s,F}$ make a step change. The asterisk marks the first operating point and the dot the second one considered after the control action at $t = 0.27$ h = 16.2 min.

RESULTS FOR DAF THICKENING WITH SEDIMENTATION

For the case study of a DAF thickener in Figure 2, we have used the constant cross-sectional area $A = \pi\, 2.5^2$ m^2 = 19.635 m^2, height H =2 m and feed inlet at $z_F = 1$ m.

Scenario DAF1

We simulate a DAF tank that initially contains only water and the feed volume fractions are $\phi_F = 0.2$ and $\phi_{F,s} = 0.2$. The operating chart can be seen in Figure 6 (left). Choosing the operating point $(Q_U, Q_F) = (300,\ 450)$ m^3/h in the white region, one gets the simulation shown in Figure 7. A first desired steady state, with aggregates only above the feed inlet and solids only below it, appears quickly after about $t = 0.07$ h = 4.2 min. Then, we change the feed volume fraction of aggregates from $\phi_F = 0.2$ to $\phi_F = 0.4$ and simulate the reaction of the system; see Figure 7(a) and 7(b). As Figure 7(a) shows, aggregates accumulate at the top of the vessel and a growing layer reaches and passes below the feed point. In the corresponding operating chart for this new set of variables, in Figure 6 (right), the operating point, marked with an asterisk, lies now outside the admissible white region. To avoid this situation, we resimulate the scenario and perform a control action at $t = 0.27$ h = 16.2 min by choosing a new operating point $(Q_U, Q_F) = (250,\ 600)$ m^3/h inside the white area in Figure 6 (right), marked with a dot. In Figure 7(c) and 7(d) the reaction of the system is shown. The layer of aggregates that was increasing downwards now turns upwards, eventually leaving through the effluent. In this case, a desired steady state is finally reached after $t = 0.5$ h = 30 min.

Scenario DAF2

In this second example, we focus on the solids behaviour. We consider solid particles whose density is slightly larger than that of water so they can easily be caught in an upstream towards the effluent. To simulate this, we choose the lower value $v_{term,s} = 0.1$ cm/s and consider a tank initially filled with water when aggregates and solids are fed with volume fractions $\phi_F = 0.3$ and $\phi_{F,s} = 0.1$. The point $(Q_U, Q_F) = (100,\ 400)$ m^3/h is chosen in the white region of the operating chart in Figure 8, which is a necessary condition for a desired steady state, but not sufficient, as can be seen for small time periods in the simulation result in Figure 9. A steady state is quickly reached for the aggregates while solid particles start settling but also move upwards, leaving through the effluent after $t = 0.2$ h = 12 min. This is not a desired steady state. Therefore, at $t = 0.2$ h = 12 min, we make a control action by setting $(Q_U, Q_F) = (250,\ 400)$ m^3/h. Figure 9 shows how the aggregates quickly reach a desired steady state with a high concentration in the effluent while the solids that where on the upper part of the tank slowly settle to the bottom, reaching a steady state with solids present only below the feed inlet after $t = 2$ h.

DISCUSSION

We have applied the three-phase flow model to two specific tanks with specific constitutive relationships for the drift flux $j_b(\phi)$ and settling flux $f_b(\varphi)$ given by Equations (3) and (4), respectively. The generality of the model lies, however, in that any cross-sectional area function $A(z)$ can be used along with any other functional form for both the drift-flux $j_b(\phi)$ and the settling-flux function $f_b(\varphi)$. The determination of which functional form to use and how to calibrate the parameters is a topic of its own, not dealt with here. The rise velocity of aggregates depends on the sizes of the air bubbles, the density of the attached particles and the aggregate concentration in the mixture. The rise velocity of activated sludge can be controlled by addition of coagulants/flocculants, which leads to different drift-flux relationships (Dockko *et al.* 2006). In other words, the parameters in Equation (3) (or another function) depend on the polymer dosage to flocculate the activated sludge before it enters the tank.

An operating chart for a DAF process gives an admissible region where the operating point (Q_U, Q_F) has to lie to obtain a desired steady state. This is, however, a necessary condition in the following meaning. Depending on the distribution of aggregates and solids in the tank at a certain time

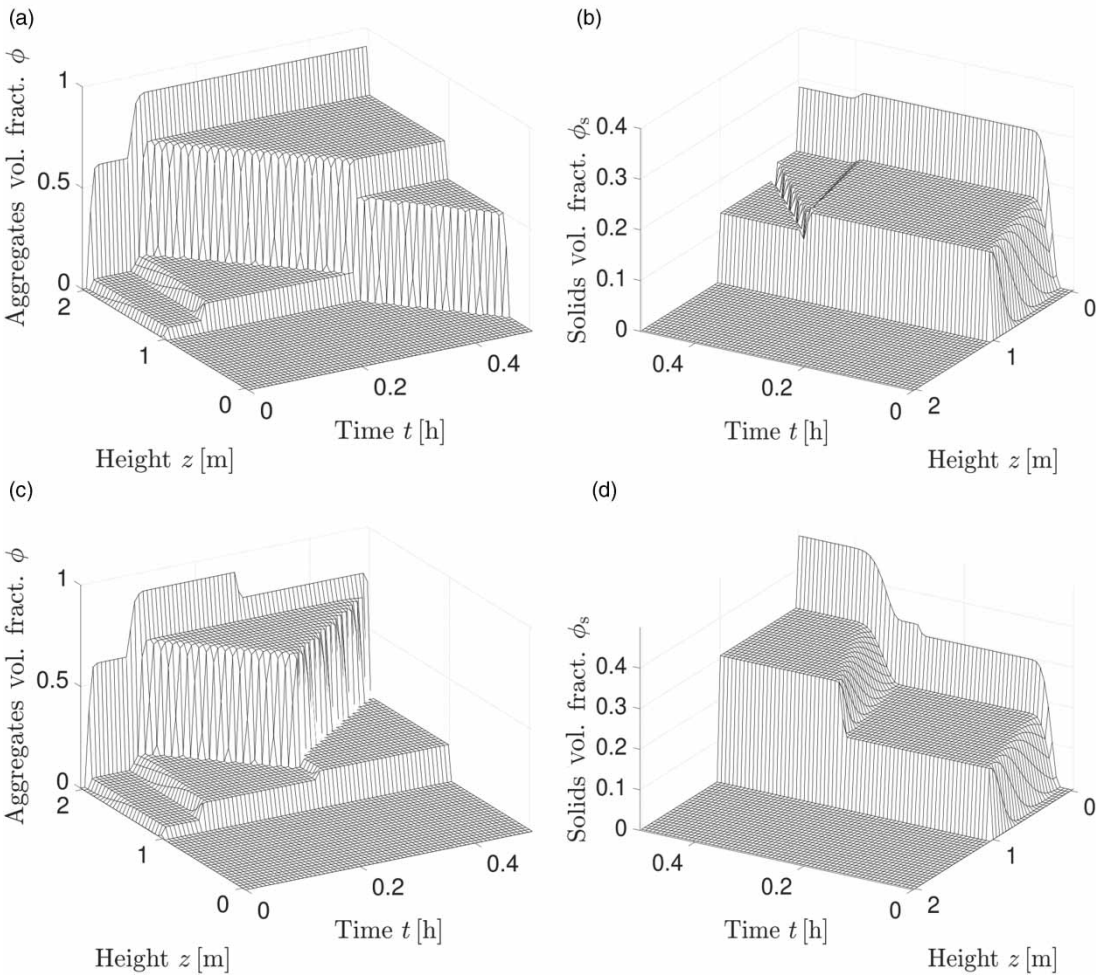

Figure 7 | Scenario DAF1: the first row shows a simulation of aggregates (a) and solids (b) volume fraction without control action. A layer of aggregates is built up and grows into the thickening zone below the feed level (zone 1). The second row (c, d) shows a simulation with control action at $t = 0.27$ h $= 16.2$ min.

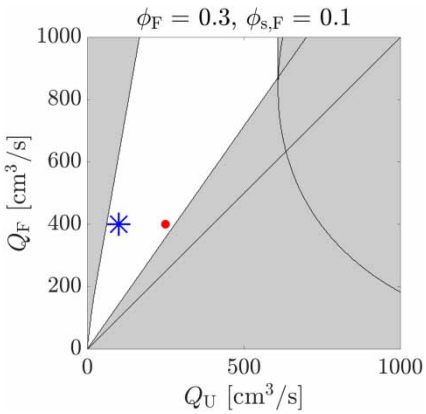

Figure 8 | Scenario DAF2: operating chart for feed volume fractions of aggregates $\phi_F = 0.3$ and solids $\phi_{s,F} = 0.1$. The asterisk marks the first operating point and the dot the second one considered after the control action.

point, one may have to perform several control actions where the last of them is to choose (Q_U, Q_F) in the admissible region. On the other hand, if (Q_U, Q_F) lies *outside* the admissible region, a desired steady state cannot be attained. In extreme or badly operated situations when the process is over- or underloaded, the model does not break down; hence, it is robust.

Another salient feature of the model is the inclusion of sedimentation of hydrophilic particles in the liquid outside the aggregate bubbles. The model and the operating chart become particularly important if the density of the particles is only slightly larger than that of water, which we have demonstrated in Scenario DAF2.

CONCLUSIONS

Thanks to recent mathematical research related to the theory and numerical analysis for hyperbolic PDEs with

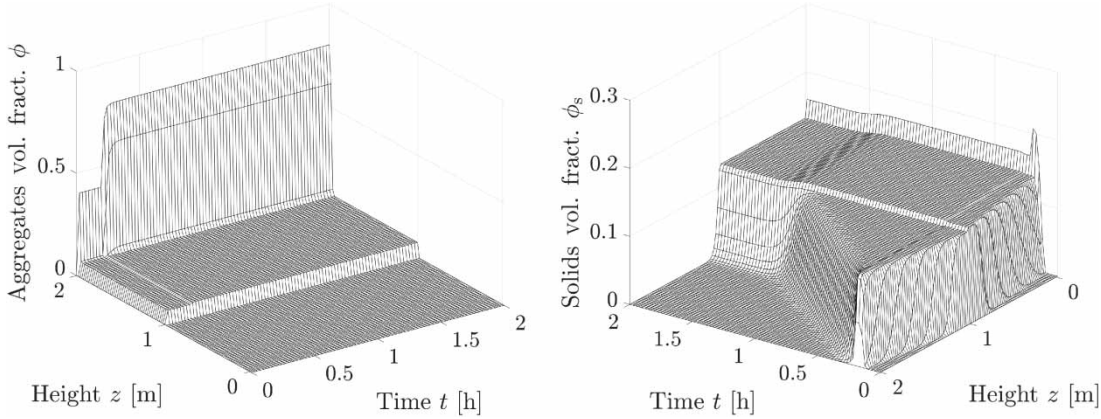

Figure 9 | Scenario DAF2: simulation of aggregates (left) and solids (right) volume fraction with a control action taken at $t = 0.2$ h $= 12$ min. The final steady state has a desired large jump in the volume fraction of aggregates at the top of the tank and all slowly settling particles leave through the underflow.

discontinuous flux functions, the three-phase flow of rising aggregates and settling particles in a fluid can be modelled and simulated with several inlets and outlets. Consequently, the model can be used for flotation/sedimentation applications which can be modelled in 1D. We have exemplified that the appearance of a layer of foam at the top, which is needed in some applications, is a natural consequence of constitutive functions used in the model. Hence, there is no need to add extra equations for the tracking of the froth/pulp interface.

A concrete outcome is that the DAF thickening process with additional sedimentation of particles can be simulated dynamically and its stationary operation controlled via an operating chart that visualizes a region of admissible values of the volumetric control flows of the feed and of the underflow.

The model is based on the simplifying assumption that the aggregation process has been completed before the mixture is fed into the vessel. In the future, we intend to include the more realistic case that aggregation may occur within the vessel as the bubbles rise. The aggregation process is difficult to model; see, e.g., Fukushi *et al.* (1995). Then at least one additional PDE has to be added keeping track of the level of aggregation of the bubbles as function of time and height. Another extension is to include compression effects at high concentrations.

ACKNOWLEDGEMENTS

R.B. acknowledges support by Fondecyt project 1170473; CONICYT/PIA/ AFB170001; CRHIAM, Proyecto ANID/ Fondap/15130015; and by the INRIA Associated Team 'Efficient numerical schemes for non-local transport phenomena' (NOLOCO; 2018-2020). M.C.M. is supported by Spanish MINECO grant MTM2017-83942-P. Y.V. is supported by SENACYT (Panama).

REFERENCES

Bascur, O. A. 1991 A unified solid/liquid separation framework. *Fluid/Part. Sep. J.* **4**, 117–122.

Bascur, O. A. 2011 A flotation model framework for dynamic performance monitoring. In: *International Mineral Processing Seminar, PROCEMIN 2011* (R. Kuyvenhoven, ed.). Gecamin, Santiago, Chile.

Beheir, S. G. & Aziz, M. 1996 Removal of Zn(II) from dilute aqueous solutions and radioactive process wastewater by foam separation. *J. Radioanal. Nucl. Chem.* **209**, 75–89.

Bratby, J. R. & Ambrose, W. A. 1995 Design and control of flotation thickeners. *Water Sci. Technol.* **31** (3–4), 247–261.

Bürger, R., Diehl, S., Farås, S., Nopens, I. & Torfs, E. 2013 A consistent modelling methodology for secondary settling tanks: a reliable numerical method. *Water Sci. Technol.* **68** (1), 192–208.

Bürger, R., Diehl, S. & Martí, M. C. 2018 A conservation law with multiply discontinuous flux modelling a flotation column. *Networks Heterogen. Media* **13**, 339–371.

Bürger, R., Diehl, S. & Martí, M. C. 2019 A system of conservation laws with discontinuous flux modelling flotation with sedimentation. *IMA J. Appl. Math.* **84**, 930–973.

Bürger, R., Diehl, S., Martí, M. C. & Vásquez, Y. Flotation with sedimentation: steady states and numerical simulation of transient operation. *Miner. Eng.*, in press.

Butler, R. C., Finger, R. E., Pitts, J. F. & Strutynski, B. 1997 Advantages of cothickening primary and secondary sludges in dissolved air flotation thickeners. *Water Environ. Res.* **69**, 311–316.

Chavadej, S., Phoochinda, W., Yanatatsaneejit, U. & Scamehorn, J. F. 2004 Clean-up of oily wastewater by froth flotation: effect

of microemulsion formation III: use of anionic/nonionic surfactant mixtures and effect of relative volumes of dissimilar phases. *Sep. Sci. Technol.* **39** (13), 3097–3112.

Chung, T. H. & Kim, D. Y. 1997 Significance of pressure and recirculation in sludge thickening by dissolved air flotation. *Water Sci. Technol.* **36** (12), 223–230.

Cruz, E. B. 1997 *A Comprehensive Dynamic Model of the Column Flotation Unit Operation*. PhD thesis, Virginia Tech, Blacksburg, VA, USA.

Dickinson, J. E. & Galvin, K. P. 2014 Fluidized bed desliming in fine particle flotation – part I. *Chem. Eng. Sci.* **108**, 283–298.

Diehl, S. 1996 A conservation law with point source and discontinuous flux function modelling continuous sedimentation. *SIAM J. Appl. Math.* **56**, 388–419.

Diehl, S., Sparr, G. & Olsson, G. 1990 Analytical and numerical description of the settling process in the activated sludge operation. In: *Instrumentation, Control and Automation of Water and Wastewater Treatment and Transport Systems* (R. Briggs, ed.). Pergamon Press, Oxford, UK, pp. 471–478.

Dockko, S., Park, S. C., Kwon, S. B. & Han, M. Y. 2006 Application of the flotation process to thicken the sludge from a DAF plant. *Water Sci. Technol.* **53** (7), 159–165.

Droste, R. & Gehr, R. 2019 *Theory and Practice of Water and Wastewater Treatment*, 2nd edn. Wiley, Hoboken, NJ, USA.

Finch, J. A. & Dobby, G. S. 1990 *Column Flotation*. Pergamon Press, London, UK.

Fukushi, K., Tambo, N. & Matsui, Y. 1995 A kinetic model for dissolved air flotation in water and wastewater treatment. *Water Sci. Technol.* **31** (3–4), 37–47.

Galvin, K. P. & Dickinson, J. E. 2014 Fluidized bed desliming in fine particle flotation – part II: flotation of a model feed. *Chem. Eng. Sci.* **108**, 299–309.

Haarhoff, J. & Bezuidenhout, E. 1999 Full-scale evaluation of activated sludge thickening by dissolved air flotation. *Water SA* **25** (2), 153–166.

Howe, K. J., Hand, D. W., Crittenden, J. C., Trussell, R. R. & Tchobanoglous, G. 2012 *Principles of Water Treatment*. Wiley, Hoboken, NJ, USA.

Karlsen, K. H., Mishra, S. & Risebro, N. H. 2009 Convergence of finite volume schemes for triangular systems of conservation laws. *Numer. Math.* **111**, 559–589.

Lin, S. H. & Lo, C. C. 1996 Treatment of textile wastewater by foam flotation. *Environ. Technol.* **17** (8), 841–849.

MATLAB 2019 *Release 2019b*. The MathWorks Inc., Matick, MA, USA.

Metcalf & Eddy 2014 *Wastewater Engineering: Treatment and Resource Recovery*, 5th edn. McGraw-Hill, New York, USA.

Peng, W., Han, G., Cao, Y., Sun, K. & Song, S. 2018 Efficiently removing Pb(II) from wastewater by graphene oxide using foam flotation. *Colloids Surf. A* **556**, 266–272.

Qian, S., Wu, W., Zheng, H. & Geng, Y. 2009 Study on riboflavin recovery from wastewater by a batch foam separation process. *Sep. Sci. Technol.* **44** (11), 2681–2694.

Reali, M., Patrizzi, L. J. & Cordeiro, J. S. 2005 Comparison of thickening of sludges produces in two water treatment plants by using DAF and gravity. *Minerva* **2** (2), 195–201.

Richardson, J. F. & Zaki, W. N. 1954 Sedimentation and fluidization: part I. *Trans. Inst. Chem. Eng.* **32**, 35–53.

Rubio, J., Souza, M. L. & Smith, R. W. 2002 Overview of flotation as a wastewater treatment technique. *Miner. Eng.* **15**, 139–155.

Saththasivam, J., Loganathan, K. & Sarp, S. 2016 An overview of oil–water separation using gas flotation systems. *Chemosphere* **144**, 671–680.

Wallis, G. B. 1969 *One-Dimensional Two-Phase Flow*. McGraw-Hill, New York, USA, p. 281.

Wang, L. K., Shammas, N. K., Selke, W. A. & Aulenbach, D. B. 2007 Flotation thickening. In: *Biosolids Treatment Processes. Handbook of Environmental Engineering*, Vol. 6 (L. K. Wang, N. K. Shammas & Y. T. Hung, eds). Humana Press, Totowa, NJ, USA.

First received 2 October 2019; accepted in revised form 19 May 2020. Available online 29 May 2020